

## ARTICLE OPEN



# Single- and multi-year ENSO events controlled by pantropical climate interactions

Ji-Won Kim<sup>1,2</sup> and Jin-Yi Yu<sup>1</sup>

To better understand the diverse temporal evolutions of observed El Niño–Southern Oscillation (ENSO) events, which are characterized as single- or multi-year, this study examines similar events in a 2200-year-long integration of Community Earth System Model, version 1. Results show that selective activation of inter- and intra-basin climate interactions (together, pantropical climate interactions) controls ENSO's evolution pattern. When ENSO preferentially activates inter-basin interactions with tropical Indian and/or Atlantic Oceans, it introduces negative feedbacks into the ENSO phase, resulting in single-year evolution. When ENSO preferentially activates intra-basin interactions with subtropical North Pacific, it causes positive feedbacks, producing multi-year evolution. Three key factors (developing-season intensity, pre-onset Pacific condition, and maximum zonal location) and their thresholds, which determine whether inter- or intra-basin interactions are activated and whether an event will become a single- or multi-year event, are identified. These findings offer a way to predict ENSO's evolution pattern by incorporating the controlling role of pantropical climate interactions.

*npj Climate and Atmospheric Science* (2022)5:88; <https://doi.org/10.1038/s41612-022-00305-y>

## INTRODUCTION

No two El Niño–Southern Oscillation (ENSO) events are alike<sup>1</sup>. Instead, considerable spatiotemporal differences appear from one event to another and asymmetries exist between the warm El Niño and cold La Niña phases of ENSO (often referred to as ENSO complexity)<sup>2</sup>. Understanding the complex interevent ENSO behaviors and their underlying mechanisms has been a central topic for ENSO research in the past decade<sup>3–13</sup>.

Regarding ENSO's temporal evolution, it is frequently observed that the event-to-event evolutions of El Niño and La Niña deviate significantly from their theoretical symmetric, regular oscillation mode<sup>14,15</sup>, which is manifested in part by the asymmetric, irregular ENSO oscillation, with El Niños terminating earlier after their peak than La Niñas, on average, as the latter last two years or longer<sup>16–22</sup>. However, it is also observed that, despite less frequent than La Niñas, some El Niños persist longer after one year and sometimes re-intensify to become a multi-year El Niño event, such as the 2014–2016 event<sup>23</sup>. Since then, researchers have begun to more focus on understanding the diverse ENSO evolution patterns<sup>23–28</sup>: An El Niño event can be followed by an opposite La Niña condition in the second year, or vice versa, resulting in a transitional single-year ENSO evolution pattern. Alternatively, an El Niño can be followed by another El Niño condition in the second year and vice versa for a La Niña, producing a successive multi-year ENSO evolution pattern. The multi-year evolution pattern can be further divided into a lingering or re-intensified multi-year evolution pattern<sup>23</sup>.

It has been increasingly recognized that ENSO's temporal evolution, which is inherently anchored in the tropical Pacific Ocean, is also tightly linked with the climate feedbacks from the neighboring Indian and Atlantic Oceans<sup>29</sup>. Anomalous Indian and Atlantic sea surface temperatures (SSTs) induced by El Niño, which occasionally amplify the El Niño's growth rate<sup>30</sup>, can both accelerate the demise of the El Niño and facilitate its phase transition through the 'inter-basin' climate interactions<sup>31–37</sup>. By

enhancing the northwest Pacific anomalous anticyclone during the mature and decay stages of the El Niño, the SST anomalies (SSTAs) in the Indian and Atlantic Oceans can drive easterly anomalies over the equatorial western Pacific which exert negative feedbacks on the El Niño via eastward-propagating upwelling oceanic Kelvin waves, expediting its demise. Although it seems less robust than El Niño, similar climate interactions between ocean basins also work for La Niña<sup>33,38,39</sup>. Therefore, these inter-basin interactions exert negative feedbacks on ENSO and contribute to the production of single-year ENSO events.

In addition, researchers have paid attention to the 'intra-basin' climate interactions within the same Pacific basin between tropics and subtropics since they also have considerable contributions to the ENSO evolution complexity<sup>21–23,25,28,40–43</sup>. During El Niño, large, warm SSTAs are often induced in the subtropical north-eastern Pacific as a result of the El Niño's atmospheric teleconnection to the extratropics<sup>44,45</sup>. These El Niño-induced subtropical SSTAs can then spread back into the equatorial central Pacific via the so-called wind–evaporation–SST (WES) feedback<sup>46</sup> and/or trade wind charging (TWC) mechanism<sup>47</sup> and exert positive ENSO feedbacks to trigger another El Niño, leading to a multi-year El Niño<sup>21,23,28,40–42</sup>. Similar intra-basin processes also work during La Niña<sup>21,22</sup>. Therefore, in contrast to the inter-basin interactions, the intra-basin interactions exert positive feedbacks on ENSO to help produce multi-year ENSO events.

The above findings collectively suggest that the inter- and intra-basin interactions occurring throughout all tropics and the neighboring subtropics (as a whole, hereafter referred to as 'pantropical' climate interactions following Cai et al.<sup>29</sup> but expanding the meaning to further include the intra-basin interactions) play crucial but possibly different roles in controlling ENSO's temporal evolution and thus its complexity. Nonetheless, it is unclear what determines whether the negative or positive ENSO feedbacks from the inter- or intra-basin interactions would dominate during an ENSO event and lead to a particular evolution

<sup>1</sup>Department of Earth System Science, University of California, Irvine, CA, USA. <sup>2</sup>Present address: Jet Propulsion Laboratory, California Institute of Technology, Pasadena, CA, USA. ✉email: [jiwok13@uci.edu](mailto:jiwok13@uci.edu)

pattern. Do certain correlations exist between ENSO properties and relative strengths of these pantropical climate interactions? A better understanding of the controlling factors for the pantropical climate interactions has the potential to greatly help predict whether an ENSO event will terminate shortly after one year as a single-year event, or last two years or longer as a multi-year event. In this study, we analyze a 2200-year-long integration produced by the Community Earth System Model, version 1 (CESM1)<sup>48</sup>, which has been proven to realistically simulate the observed complex ENSO behaviors including the diverse evolution patterns<sup>23,26,28,49</sup>, in order to better understand the roles of the pantropical climate interactions in shaping ENSO's temporal evolution and identify key factors separating ENSO events into single- and multi-year events.

## RESULTS

### Evolution characteristics of single- and multi-year ENSO

We first identified single- and multi-year ENSO events in the observations during 1900–2020 and in the CESM1 simulation during model years of 400–2200 (Supplementary Table 1; see Methods). The sample sizes of single- and multi-year ENSO events in the CESM1 are about 12–18 times larger than those in the observations (compare Fig. 1a, c, and e, g). About 54% and 46% of El Niños in the CESM1 are single- and multi-year events, respectively, which are very close to the relative percentages in the observations (i.e., 56% and 44%); about 28% and 72% of La Niñas in the CESM1 are single- and multi-year events, respectively, and their relative percentages are almost same as those in the observations (i.e., 30% and 70%) (Supplementary Fig. 1). Therefore, the CESM1 provides large sample sizes of single- and multi-year ENSO events and reproduces their relative percentages as in the observations, with El Niños becoming single-year events slightly more often but La Niñas becoming multi-year events very often.

Using the single- and multi-year ENSO events in the observations and CESM1, we performed composite analyses to examine their averaged spatiotemporal evolution characteristics. Note that the single- and multi-year ENSO events were only selected in the composite analyses when their second winter (i.e., November<sup>1</sup> to January<sup>2</sup>) Niño3.4 indices greater than  $\pm 0.25$  s.d. ( $\pm 0.23$  °C for observations and  $\pm 0.28$  °C for CESM1); otherwise, the events were excluded in the analyses (see the closed and open dots in Fig. 1a, c, e, g). This additional threshold filters out events that have neutral-ENSO conditions in the second year from being counted as single- or multi-year events. Therefore, it increases the contrasting evolution characteristics between single- and multi-year ENSO events and makes them more distinguishable (Supplementary Fig. 2). The Niño3.4 temporal evolutions in the observations (Fig. 1b, d) clearly show that single-year ENSO events decay abruptly after their peak stage and transition their phase around the summer of decaying year. However, multi-year ENSO events do not transition their phase after their peak stage but instead persist in the same sign during the subsequent seasons and re-intensify in around the winter of decaying year. The longitude-time plots of equatorial Pacific SSTAs (Fig. 1i–l) support the abovementioned evolution characteristics of single- and multi-year ENSO events as they exhibit a stark contrast in their decay evolutions. It is also noticeable that the peak of single-year El Niño, on average, has a stronger intensity than the 1<sup>st</sup>-year peak of multi-year El Niño (Fig. 1b, i, j), and its maximum SSTAs are located further into the tropical eastern Pacific (see white circled dots in Fig. 1i, j). These contrasts imply that the single-year El Niño is more related to the Eastern Pacific (EP) El Niño dynamics whereas the multi-year El Niño is more linked to the Central Pacific (CP) El Niño<sup>3</sup> dynamics<sup>21–23,50</sup>. For La Niña, the composites inversely indicate that the 1<sup>st</sup>-year peak of multi-year La Niña has a stronger intensity than that of single-year La Niña (Fig. 1d, k, l). Similar to

the El Niño, the maximum SSTAs (i.e., minimum cold SSTAs) are located more into the tropical eastern Pacific for single-year La Niña but more into the tropical central Pacific for multi-year La Niña (see white crossed dots in Fig. 1k, l).

We also performed similar composite analyses with the single- and multi-year ENSO events in the CESM1. It is evident from the Niño3.4 index evolutions (Fig. 1f, h) and longitude-time plots (Fig. 1m–p) that the model realistically simulates the key evolution features from the observed single- and multi-year ENSO events, which include the contrasting evolution patterns during their decaying year and differences in their intensities and maximum zonal locations. The CESM1, however, also has some disagreements with the observations as below. Firstly, compared to the observations, the simulated multi-year El Niño tends to have its 2<sup>nd</sup>-year peak intensity stronger than its 1<sup>st</sup>-year peak intensity (compare red curves in Fig. 1b, f). This is presumably due to model characteristics that lead the CESM1 to frequently produce the re-intensified type of multi-year El Niño that begins with a 1<sup>st</sup>-year weak equatorial Pacific warming followed by a rapid re-intensification in the second year<sup>23,26,51</sup>. The second is that, while the observed La Niñas are preceded by an El Niño condition<sup>52</sup> for both the single- and multi-year events (Fig. 1d, k, l), a similar preceding El Niño condition exists only for the multi-year La Niña but not for the single-year La Niña in the CESM1 (Fig. 1h, o, p). Nonetheless, it is also noticeable from the observations that the preceding El Niño condition is weaker for single-year La Niña than multi-year La Niña. The pre-onset Pacific condition difference between single- and multi-year La Niñas appears to be amplified in the CESM1. This difference, as will be shown later, is one key factor to determine whether a La Niña should develop into a single- or multi-year evolution pattern.

### Pantropical climate interactions that control ENSO evolution

To explore how the pantropical climate interactions and the diverse ENSO evolutions are dynamically linked, we contrasted the composite seasonal evolutions of SST and surface wind anomalies between single- and multi-year ENSO events in the CESM1. For the single-year El Niño (Fig. 2a), its inter-basin interactions are characterized (i) in the Indian Ocean by a positive phase of the Indian Ocean Dipole (IOD)<sup>53</sup> during the developing summer/fall and a basin-scale SST warming of the Indian Ocean Basin (IOB) mode<sup>54</sup> during the following winter/spring; and (ii) in the Atlantic Ocean by another basin-scale SST warming particularly over the tropical North Atlantic (TNA) during the peak winter and decaying spring<sup>55</sup>. Those are known as the typical El Niño teleconnections to the neighboring oceans and their underlying physical mechanisms have been well understood<sup>29</sup>. As mentioned in the Introduction, these SSTAs in the neighboring Indian and Atlantic Oceans driven by El Niño teleconnections, in turn, exert negative ENSO feedbacks to terminate the El Niño and transition its phase into La Niña during the decaying summer, resulting in a single-year evolution pattern.

Differently from the single-year El Niño, the multi-year El Niño (Fig. 2b) induces weak SSTAs in the Indian and Atlantic Oceans during its first ENSO cycle from the first- to second-year spring. In other words, the Indian and Atlantic SST variability (i.e., a positive IOD, IOB warming, and TNA warming), which represent the strength of the inter-basin interactions, are weakened during multi-year El Niño. The inter-basin interactions thus cannot play a role in terminating and transitioning the El Niño. However, it is not necessarily guaranteed that the weak inter-basin interactions will promote 1<sup>st</sup>-year El Niño persistence into the second year because the chief role of inter-basin interactions is to help expedite the demise of the El Niño. Instead, we here find that the intra-basin interactions within the Pacific play a role for generating a multi-year El Niño evolution pattern. During the peak winter of the 1<sup>st</sup>-year El Niño (i.e., December<sup>0</sup> to February<sup>1</sup>), an initiation of a

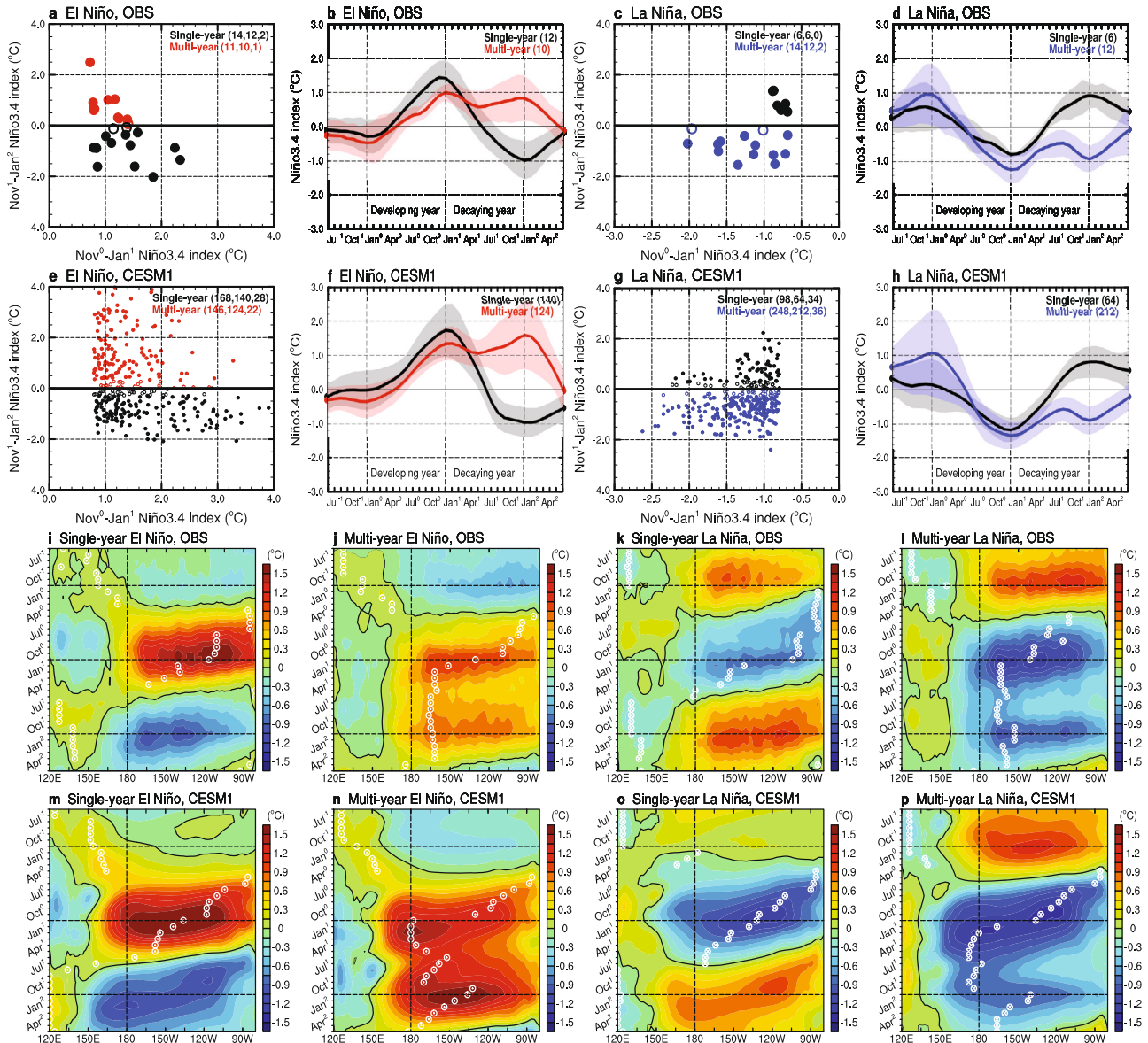


**Fig. 1** Spatiotemporal evolution characteristics of single- and multi-year ENSO events. **a** Scatter plot of the 1<sup>st</sup>-winter Niño3.4 index values against their 2<sup>nd</sup>-winter values for the El Niños in the observations. Black and red dots respectively indicate the events classified into single- and multi-year events (see Methods). The events selected for and excluded from composite analysis are expressed as closed and open dots, respectively. The numbers of total, selected, and excluded events are shown in parenthesis. **b** Temporal evolutions of the Niño3.4 index for the selected single (black curve) and multi (red curve)-year El Niños with their  $\pm 1$  standard deviations shaded. **c, d** Same as **a, b** except for single- and multi-year La Niñas with their multi-year events expressed in blue. **e–h** Same as **a–d**, respectively, except for the ENSO events in the CESM1. Longitude-time plot of equatorial (i.e., 5°S–5°N) Pacific SSTAs for the selected **i** single-year El Niño, **j** multi-year El Niño, **k** single-year La Niña, and **l** multi-year La Niña. The black contours denote zero lines and the white dots mark the longitudinal locations of maximum SSTAs for El Niños (circled dot) and La Niñas (crossed dot). **m–p** Same as **i–l**, respectively, except for the ENSO events in the CESM1.

positive phase of the Pacific Meridional Mode (PMM)<sup>56</sup> is clearly noticeable, with warm SSTAs extending from the subtropical North Pacific to the equatorial central Pacific accompanied by surface southwesterly wind anomalies in between. Recent studies, based on modeling and observational evidence, have suggested that the positive PMM is often induced by a CP El Niño which efficiently generates a subtropical atmospheric circulation anomaly near Hawaii, including the PMM region<sup>3,13,44,45,57</sup>. That is because the CP El Niño, compared to a canonical EP El Niño, more easily excites tropical convection anomalies due to its maximum SSTAs being located near the Pacific warm pool where background SSTs are already very close to the convective threshold ( $\sim 28^\circ\text{C}$ ; see magenta contour and white circled dot in Fig. 2b)<sup>58</sup>. This positive PMM is able to maintain for several seasons through

the WES feedback<sup>46</sup>, in cooperation with the TWC mechanism<sup>47</sup>, subsequently spreads its warm SSTAs into the equatorial central Pacific where the warm SSTAs are conducive to the development of another El Niño<sup>13,23,28,40–42</sup>—resulting in a multi-year evolution pattern. In contrast, the single-year El Niño has its maximum SSTAs located more into the equatorial eastern Pacific during the peak winter, further away from the Pacific warm pool (see magenta contour and white circled dot in Fig. 2a). Therefore, the El Niño cannot induce a noticeable PMM variability in the subtropical North Pacific and is solely capable of invoking such inter-basin interactions with the Indian and Atlantic Oceans (compare Fig. 2a, b and Supplementary Fig. 3a).

The bar-charts displaying seasonally-averaged climate indices (Fig. 2c; see Methods for index definitions) during El Niño provide



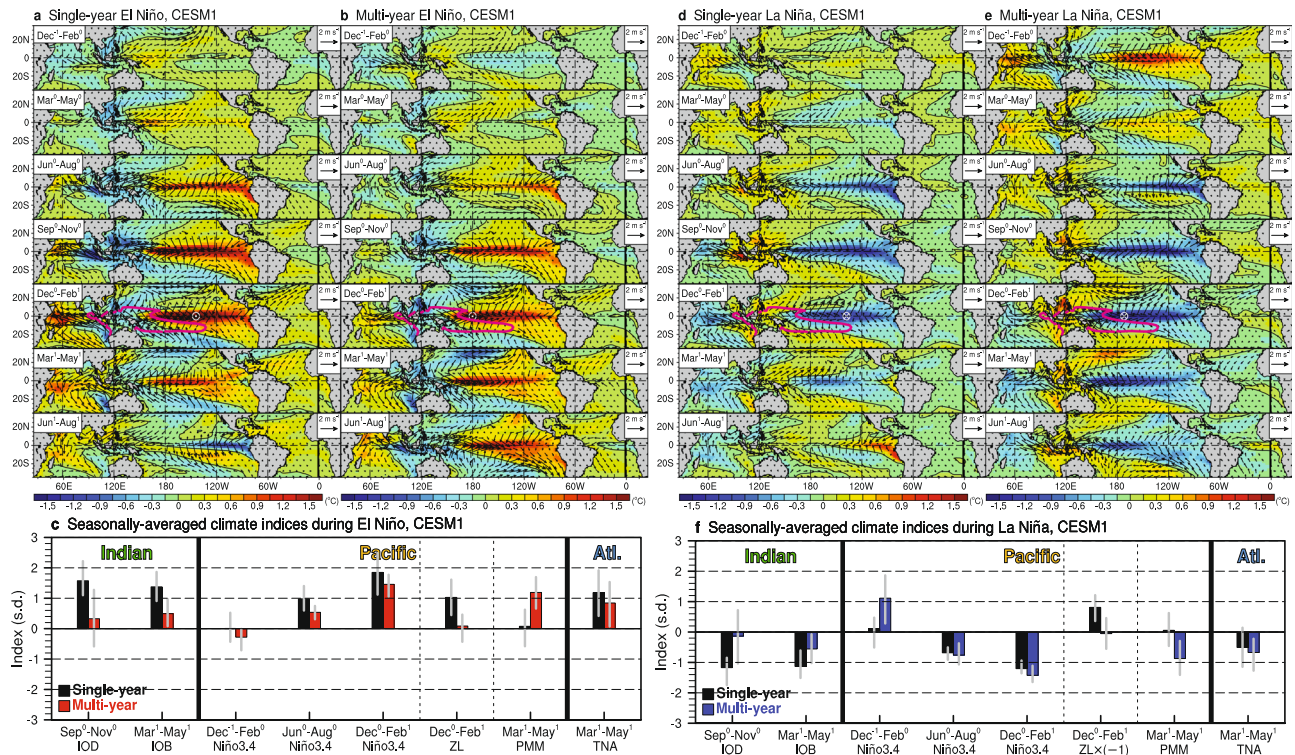


**Fig. 2** Selective activations of pantropical climate interactions during single- and multi-year ENSO events. Composite seasonal structures of anomalous SST (shading; zero values expressed in black contour) and surface wind (vector) over the entire tropics for the **a** single- and **b** multi-year El Niños in the CESM1 during their preceding winter (i.e., December<sup>1</sup> to February<sup>0</sup>), developing spring (i.e., March<sup>0</sup> to May<sup>0</sup>), summer (i.e., June<sup>0</sup> to August<sup>0</sup>), fall (i.e., September<sup>0</sup> to November<sup>0</sup>), peak winter (i.e., December<sup>0</sup> to February<sup>1</sup>), decaying spring (i.e., March<sup>1</sup> to May<sup>1</sup>), and summer (i.e., June<sup>1</sup> to August<sup>1</sup>). The magenta contours and circled/crossed dots for El Niño/La Niña during the peak winter represent climatological 28°C isotherm line and longitudinal position of the maximum SSTAs, respectively. **c** Bar-chart displaying seasonally-averaged climatological indices of IOD, IOB, Niño3.4, ZL, PMM, and TNA for the single (black bar-chart) and multi (red bar-chart)-year El Niños (see Methods for the index definitions). All the indices are normalized by their standard deviations and the gray bars indicate their interquartile ranges (that is, the 75<sup>th</sup> percentile minus the 25<sup>th</sup> percentile; see Methods). **d–f** Same as **a–c**, respectively, except for single- and multi-year La Niñas. In **f**, the bar-charts displaying multi-year La Niña are expressed in blue and the ZL index is multiplied by  $-1$ , so that its increasing (decreasing) value corresponds to a more eastward (westward)-centered La Niña location.

further and quantitative evidence that single- and multi-year El Niños invoke respectively the inter- and intra-basin interactions for their development. The climate indices of IOD, IOB, and TNA have strong positive values that are larger for single-year El Niño ( $>1$  s.d.) than multi-year El Niño—an activation of inter-basin interactions during single-year El Niño. The differences are much larger for the Indian Ocean indices (i.e., IOD and IOB) than the Atlantic Ocean index (i.e., TNA), implying that the Indian–Pacific interactions play a larger role than the Atlantic–Pacific interactions in determining the El Niño evolution. On the contrary, the PMM index has a strong positive value only for multi-year El Niño ( $>1$  s.d.) but almost zero for single-year El Niño—an activation of intra-basin interactions during multi-year El Niño.

We repeated the same composite analyses but for La Niña. The seasonal evolution plots (Fig. 2d, e) show that the single-year La Niña invokes strong inter-basin interactions with the neighboring oceans during its first ENSO cycle, which include a negative IOD and IOB cooling in the Indian Ocean, and TNA cooling in the Atlantic Ocean (Fig. 2d). Due to the negative ENSO feedbacks provided by the inter-basin interactions, the La Niña, after its peak, terminates rapidly and transitions into El Niño during the decaying summer, resulting in a single-year evolution pattern. By contrast, it is shown in Fig. 2e that the multi-year La Niña invokes strong intra-basin interactions within the Pacific as it accompanies noticeable cold SSTAs in the subtropical North Pacific during the peak winter and decaying spring, which are manifested as a negative PMM (see also Supplementary Fig. 4). Due to the positive ENSO feedbacks provided by the intra-basin interactions, the La Niña

persists its phase and re-intensifies from the decaying summer and onward, producing a multi-year evolution pattern (compare Fig. 2d, e and Supplementary Fig. 3b). The bar-charts for the single- and multi-year La Niñas (Fig. 2f) further support their selective activations of pantropical climate interactions. The IOD and IOB indices have strong negative values that are much larger for single-year La Niña ( $<-1$  s.d.) than multi-year La Niña—an activation of inter-basin interactions during single-year La Niña. We here note that the TNA index has weak negative values for both single- and multi-year La Niñas ( $\sim-0.5$  s.d.), implying that the Atlantic–Pacific inter-basin interactions (i.e., impact of TNA cooling) on the La Niña evolution is relatively minor as compared to the Indian–Pacific inter-basin interactions. As can be expected, the PMM index has a strong negative value only for multi-year La Niña ( $\sim-1$  s.d.) but almost zero for single-year La Niña—an activation of intra-basin interactions during multi-year La Niña.

### Key factors responsible for the selective activations

As mentioned in the previous sections and shown in Fig. 2a–c, the single- and multi-year El Niños have noticeable differences in their intensities and maximum locations. The single-year El Niño has stronger intensity during the developing summer (and fall) and more eastward location of maximum SSTAs during the peak winter, whereas the multi-year El Niño has weaker intensity during the developing summer and more westward location during the peak winter. The developing-summer (i.e., June<sup>0</sup> to August<sup>0</sup>) Niño3.4 and peak-winter (i.e., December<sup>0</sup> to February<sup>1</sup>) zonal

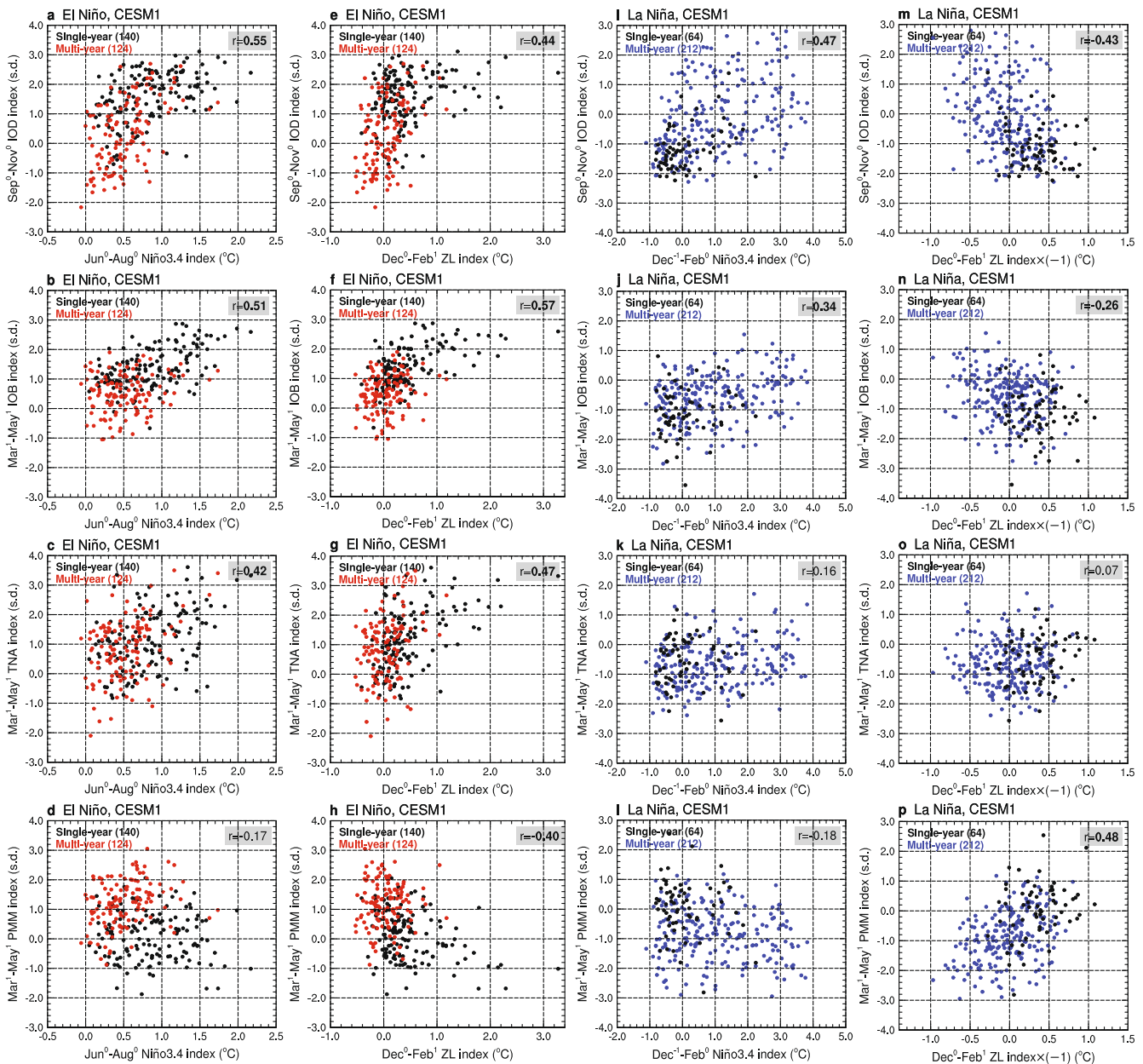


**Fig. 3 Relationships between the identified key factors and various climate indices during single- and multi-year ENSO events.** Scatter plot of developing summer Niño3.4 index (represented as developing-season intensity; 1<sup>st</sup> column) against the developing fall **a** IOD index, decaying spring **b** IOB, **c** TNA, **d** PMM indices during the single (black dots) and multi (red dots)-year El Niños in the CESM1, respectively, except for peak winter ZL index (represented as zonal maximum location; 2<sup>nd</sup> column). **i–p** Same as **a–h**, respectively, except it displays preceding winter Niño3.4 index (represented as pre-onset Pacific condition; 3<sup>rd</sup> column) and peak winter ZL index (represented as zonal maximum location, multiplied by  $-1$ ; 4<sup>th</sup> column) for single (black dots) and multi (blue dots)-year La Niñas. In each panel, a correlation coefficient is marked in the upper right corner, with a number in bold denoting statistically significant at 99.9% confidence level based on the Student's  $t$  test.

location (ZL) indices shown in Fig. 2c clearly indicate that these two key property differences between single- and multi-year El Niños are statistically significant (compare gray error bars in Fig. 2c). Prior studies have shown that the stronger the El Niño intensity, the stronger the teleconnections to the neighboring Indian and Atlantic Oceans<sup>59,60</sup>. Additionally, regarding the zonal location difference, it is also known that the EP El Niños are more capable than CP El Niños of disturbing the Walker circulation and driving atmospheric teleconnections to the Indian Ocean, as well as exciting the stationary atmospheric Rossby waves into the North Atlantic<sup>61–63</sup>. Therefore, the strong developing intensity and eastward location for single-year El Niño make it more capable of

inducing a positive IOD, IOB warming, and TNA warming, thus selectively activating the inter-basin interactions. In the same manner, the weak developing intensity and westward location for multi-year El Niño make it less capable of activating the inter-basin interactions. Instead, the westward location with its close proximity to the Pacific warm pool makes it more capable of inducing a positive PMM by exciting a subtropical North Pacific cyclonic circulation anomaly<sup>13,44,45</sup>, thus selectively activating the intra-basin interactions.

The relationships between the key property factors (developing-season intensity and maximum zonal location) and the key climate indices (IOD, IOB, TNA, and PMM indices) and between the factors



**Table 1.** Partial correlation coefficients (see Methods) between the seasonally-averaged climate indices (IOD, IOB, TNA, and PMM indices) and the indices of key property differences for El Niño (developing-summer Niño3.4 and peak-winter ZL indices) and La Niña (preceding-winter Niño3.4 and peak-winter ZL indices) phases in the CESM1.

El Niño	Jun <sup>0</sup> to Aug <sup>0</sup> Niño3.4 index	Dec <sup>0</sup> to Feb <sup>1</sup> ZL index	La Niña	Dec <sup>-1</sup> to Feb <sup>0</sup> Niño3.4 index	Dec <sup>0</sup> to Feb <sup>1</sup> ZL index×(-1)
Sep <sup>0</sup> to Nov <sup>0</sup> IOD index	<b>0.38</b>	0.12	Sep <sup>0</sup> to Nov <sup>0</sup> IOD index	<b>0.28</b>	-0.18
Mar <sup>1</sup> to May <sup>1</sup> IOB index	<b>0.31</b>	0.20	Mar <sup>1</sup> to May <sup>1</sup> IOB index	<b>0.24</b>	-0.02
Mar <sup>1</sup> to May <sup>1</sup> TNA index	<b>0.26</b>	0.21	Mar <sup>1</sup> to May <sup>1</sup> TNA index	0.03	0.02
Mar <sup>1</sup> to May <sup>1</sup> PMM index	0.13	<b>-0.36</b>	Mar <sup>1</sup> to May <sup>1</sup> PMM index	0.08	<b>0.42</b>

Values in bold indicate that the coefficients are statistically significant at 99.9% confidence level based on the Student's *t* test. The ZL index for La Niña is multiplied by -1, so that an increasing (decreasing) index value indicates more eastward (westward)-centered La Niña location.

and the occurrence of single-/multi-year El Niños can also be delineated by the scatter plots in Fig. 3. Figure 3a–d shows that the developing-season intensity (represented by the June<sup>0</sup>–August<sup>0</sup> Niño3.4 index) has strong positive correlations with the IOD ( $r = 0.55$ ), IOB ( $r = 0.51$ ), and TNA ( $r = 0.42$ ) indices but a weak correlation with the PMM index ( $r = -0.17$ ). This implies that the inter-basin interactions with the tropical Indian/Atlantic Oceans (involving the IOD, IOB, and TNA), which provide negative ENSO feedbacks, are preferred when the El Niño's developing-season intensity is large. Therefore, single-year El Niños (black dots in Fig. 3a–d) occur more frequently than the multi-year El Niños (red dots) as the intensity increases. Figure 3e–h shows that the maximum zonal location, differently from the developing-season intensity, has a noticeably significant negative correlation with the PMM ( $r = -0.40$ ). This implies that the El Niño's intra-basin interactions with the subtropical North Pacific (involving the PMM), which provide positive ENSO feedbacks, are preferred when the El Niño location is shifted westward. Multi-year El Niños (red dots in Fig. 3e–h) therefore occur more frequently than single-year El Niños (black dots) as the maximum zonal location centers westward.

For La Niña, we similarly noticed two key factors between single- and multi-year La Niñas that govern their selective activations of pantropical climate interactions as the pre-onset Pacific condition and maximum zonal location. It is apparent in Fig. 2d–f that single-year La Niña has a near-neutral ENSO condition during the preceding winter and more eastward location of maximum SSTAs during the peak winter, whereas multi-year La Niña has a strong preceding El Niño condition and more westward maximum location. The preceding-winter (i.e., December<sup>-1</sup> to February<sup>0</sup>) Niño3.4 and peak-winter ZL indices in Fig. 2f further confirm these two key differences between single- and multi-year La Niñas. As the eastward location of single-year La Niña (see magenta contour and white crossed dot in Fig. 2d) easily intensifies the Walker circulation during the developing year, this enables it to be more capable of inducing a negative IOD and IOB cooling and thus selectively activating the inter-basin interactions. In contrast, the westward location of multi-year La Niña (see magenta contour and white crossed dot in Fig. 2e) makes it more capable of inducing a negative PMM and thus selectively activating the intra-basin interactions since it brings SSTs below the convective threshold temperature in that region, switching off the deep convection over the tropical central Pacific, and easily exciting an anticyclonic circulation anomaly over the subtropical North Pacific<sup>21,22</sup>. Meanwhile, the pre-onset Pacific condition for multi-year La Niña may cancel out the La Niña-induced inter-basin interactions as the preceding strong El Niño produces noticeable

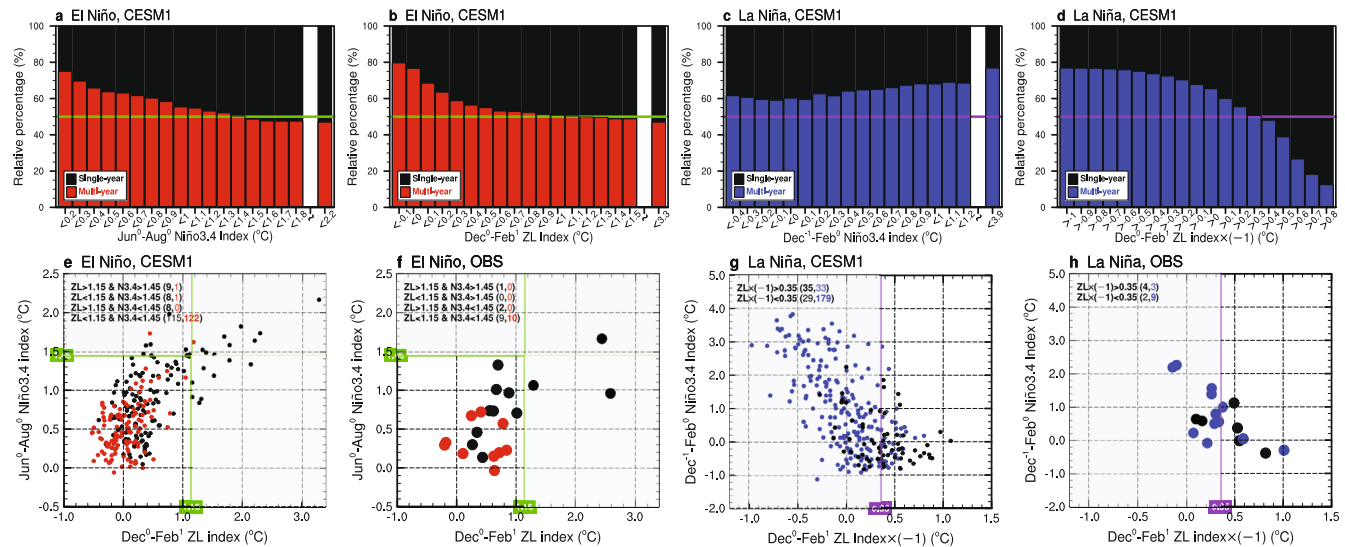
warm SSTAs in the Indian and Atlantic Oceans that lasted longer into the developing year of the 1<sup>st</sup>-year La Niña (Fig. 2e and Supplementary Fig. 3b). Such interference effects do not exist in the single-year La Niña since it has weak pre-onset Pacific condition.

Figure 3i–p supports these relationships by showing that the pre-onset Pacific condition (represented by December<sup>-1</sup>–February<sup>0</sup> Niño3.4 index) has strong positive correlations with the IOD ( $r = 0.47$ ) and IOB ( $r = 0.34$ ) indices—an indication of the preferred activation of inter-basin interactions—while the maximum zonal location (multiplied by -1) has a strong positive correlation with the PMM index ( $r = 0.48$ )—which reveals the preferred activation of intra-basin interactions. As a consequence, single-year La Niñas (black dots in Fig. 3i–p) tend to occur more frequently than multi-year La Niñas (blue dots) as the pre-onset Pacific condition weakens and vice versa as the maximum zonal location shifts westward. Here, it should be emphasized that the maximum zonal location for La Niña has received little research attention in comparison to the pre-onset Pacific condition for La Niña, which highlights a large initial heat content discharge caused by the preceding strong El Niño that often exists for multi-year La Niña<sup>26,64</sup>. This oceanic discharge view can be another reason why multi-year La Niña tends to be preceded by a strong El Niño condition, whereas single-year La Niña is not.

The abovementioned results are further supported by the partial correlation analyses that help achieve the pure relationships between the key factors and the key climate indices (see Methods). As shown in Table 1, for El Niño, the developing-summer Niño3.4 index has significant positive correlations with the seasonally-averaged IOD, IOB, and TNA indices whereas the peak-winter ZL index has a significant negative correlation with the PMM index. For La Niña, the preceding-winter Niño3.4 index has significant positive correlations with the IOD and IOB indices (except for the TNA index, further implying the minor role of the Atlantic–Pacific inter-basin interactions during La Niña), and vice versa for the peak-winter ZL index (multiplied by -1), having a significant positive correlation with the PMM index. Note that the IOD, IOB, TNA, and PMM indices used can be considered independent predictors as most correlation coefficients between them are statistically insignificant (Supplementary Table 2).

### Thresholds of the key factors and their implication

We further examined the previously identified key factors to see if they have certain thresholds that can help determine diverse ENSO evolutions in advance. The threshold value for a key factor is identified as the value of the factor with which the relative



**Fig. 4** Thresholds of the identified key factors and their implication for ENSO prediction. **a, b** Relative percentages of the single (black bar-chart) and multi (red bar-chart)-year El Niños in the CESM1 with their key factors of developing-season intensity changing from 2.2 to 0.2 °C and zonal maximum location changing from 3.3 to  $-0.1$  °C. **c, d** Same as **a, b** except for single (black bar-chart) and multi (blue bar-chart)-year La Niñas with their key factors of pre-onset Pacific condition changing from 3.9 to  $-0.4$  °C and zonal maximum location changing from  $-1.0$  to 0.8 °C. The green and purple horizontal lines in **a–d** mark a 50% relative percentage for identifying thresholds from the key factors. **e, f** Scatter plots of the zonal maximum location against the developing-season intensity for the single (black dots) and multi (red dots)-year El Niños in the CESM1 and observations. The numbers of single- and multi-year El Niños in the four regimes separated by two thresholds (two green lines) are, respectively, shown as black and red text in the legend with larger numbers in bold. **g, h** Same as **e, f** except they display the zonal maximum location against the pre-onset Pacific condition for single (black dots) and multi (blue dots)-year La Niñas with the two regimes separated by one threshold (one purple line). Gray shadings in **e–h** indicate regimes where the major ENSO group (single-year event for El Niño or multi-year event for La Niña) is dominant.

percentage of the ‘minor’ ENSO group (multi-year event for El Niño or single-year event for La Niña) begins to exceed 50%. This threshold definition makes it possible to find a certain value that reveals a regime in which the minor ENSO group begins to occur more than the major ENSO group as the factor value changes. In Fig. 4a, the relative percentage of the multi-year El Niño (the minor group of El Niño) begins to exceed 50% when the developing-season intensity varies within a range of 1.4–1.5 °C. The threshold value for this factor is thus simply identified as the midpoint value of this interval, which is 1.45 °C. The bar-charts clearly indicate that an El Niño with its developing-season intensity weaker than 1.45 °C has a larger probability of developing into a multi-year event, with its occurrence frequency sharply increasing as the intensity weakens (up to about 75% of multi-year El Niño; see red bar-charts in Fig. 4a). Similarly, as shown in Fig. 4b, the threshold that enables us to use the maximum zonal location for determining the El Niño evolution is 1.15 °C. When an El Niño has its maximum center located more westward (e.g., ZL index  $< 1.15$  °C), the El Niño has larger probability of becoming a multi-year event. The occurrence frequency also sharply increases as the location moves further westward (up to about 80% of multi-year El Niño; see red bar-charts in Fig. 4b). For La Niña, based on Fig. 4d, its threshold for the maximum zonal location can be identified as 0.35 °C, meaning that when the center of La Niña is located more eastward (e.g., ZL index  $\times (-1) > 0.35$  °C), the single-year La Niña (the minor group of La Niña) occurs more frequently than the multi-year La Niña (the major group of La Niña). Meanwhile, we cannot identify a threshold for the pre-onset Pacific condition because the relative percentage of single-year La Niña does not exceed 50% (Fig. 4c). Although the relative percentage of single-year La Niña gradually increases as the pre-onset Pacific condition weakens from positive (3.9 °C) to negative ( $-0.4$  °C) values, it reaches a plateau without exceeding 50%, holding at around 40% (see black bar-charts in Fig. 4c). This may indicate that the role of the pre-onset Pacific condition is not as critical as that of the

maximum zonal location in determining the La Niña evolution pattern.

The thresholds identified here can be useful to help determine whether an ENSO event will become a single- or multi-year event. We find in Fig. 4e that almost all El Niños occurring in the regime where either of two key factor values (the developing-season intensity and zonal maximum location) is above its threshold are single-year events ( $\sim 93\%$ ; 25 of 27 events; see gray shading area). Contrastingly, a majority of El Niños occurring in the regime where their key factor values are both below their thresholds are multi-year events ( $\sim 51\%$ ; 122 of 237 events) and this dominance of multi-year event sharply increases as the key factor values shift further below their thresholds (see red dots). For La Niña, it is similarly found in Fig. 4g that most La Niñas occurring in the regime where their zonal maximum location values are below their threshold are multi-year events ( $\sim 86\%$ ; 179 of 208 events; see gray shading area). However, a majority of La Niñas occurring in the opposite regime are single-year events ( $\sim 51\%$ ; 35 of 68 events) and its dominance also abruptly increases as the key factor value shifts further above its threshold (see black dots).

Lastly, we extended our analysis to the observed ENSO events to examine whether the thresholds we identified from the CESM1 analysis can also help determine the single- and multi-year events in the observations. Despite their limited sample sizes, there is an overall consensus in both the observed El Niños (Fig. 4f) and La Niñas (Fig. 4h) that the thresholds are helping to determine a single- or multi-year evolution pattern as the dominance of single- or multi-year event changes depending on the regimes separated by the thresholds. In addition, we also note that the results from the observations have a close resemblance to those from the CESM1 in separating the single- and multi-year ENSO events, with regards to the key factors of the developing-season intensity for El Niño (Fig. 1b, i, j), pre-onset Pacific condition for La Niña (Fig. 1d, k, l), and maximum zonal location for both El Niño and La Niña (Fig. 1i–l; see also Supplementary Fig. 5). Although further studies are required, this implies that the thresholds here can also be applied

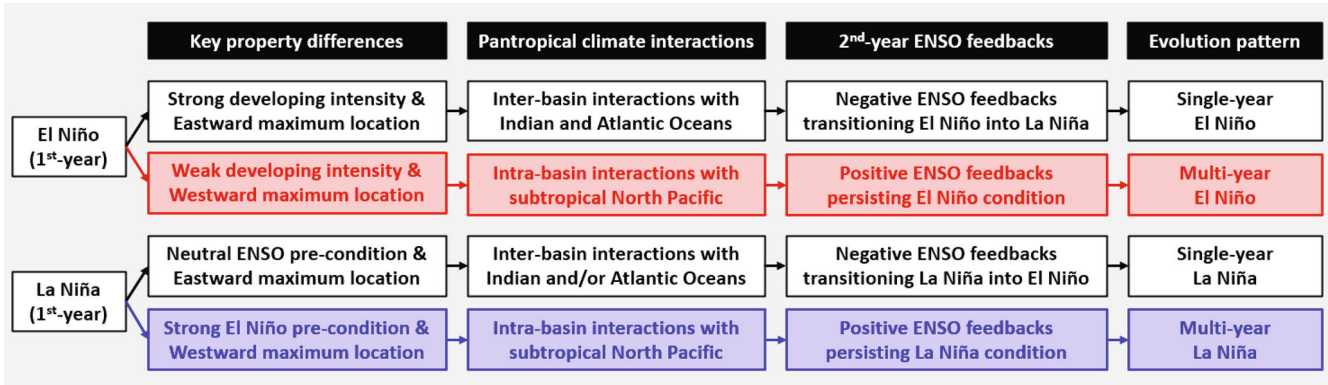


**Fig. 5 Schematic diagram illustrating how the 1<sup>st</sup>-year ENSO event evolves into either a single- or multi-year evolution event in the second year.** In the diagram, key processes determining the evolution pattern of 1<sup>st</sup>-year El Niño (two upper panels; the pathway for multi-year El Niño expressed in red) and 1<sup>st</sup>-year La Niña (two bottom panels; the pathway for multi-year La Niña expressed in blue) are sequentially categorized as ‘Key property differences’, ‘Pantropical climate interactions’, ‘2<sup>nd</sup>-year ENSO feedbacks’, and ‘Evolution pattern’.

to operational ENSO prediction and, more particularly, to improving the predictability of ‘multi-year’ El Niño and La Niña events, which still remains challenging<sup>65,66</sup>.

## DISCUSSION

In this study, we analyzed observations and a long-term (i.e., 2200 years) CESM1 simulation to better understand how ENSO events that have diverse evolution patterns—namely, single- and multi-year events—can be controlled by pantropical climate interactions. The schematic diagram displayed in Fig. 5 summarizes our main findings. The schematic illustrates which ‘Key property differences’ (boxes in the 1<sup>st</sup> column) determine what type of ‘Pantropical climate interactions’ (boxes in the 2<sup>nd</sup> column) should be activated to provide positive or negative ‘2<sup>nd</sup>-year ENSO feedbacks’ (boxes in the 3<sup>rd</sup> column) and give rise to a single-/multi-year ‘Evolution pattern’ (boxes in the 4<sup>th</sup> column). For El Niño, strong (weak) developing-season intensity and eastward (westward) maximum location favorably activate the inter-basin (intra-basin) interactions and the associated 2<sup>nd</sup>-year negative (positive) feedbacks to develop the El Niño into a single-year (multi-year) event. For La Niña, neutral ENSO (strong El Niño) pre-condition and eastward (westward) maximum location preferably activate the inter-basin (intra-basin) interactions and the associated 2<sup>nd</sup>-year negative (positive) feedbacks to develop the La Niña into a single-year (multi-year) event. These findings may enable us to use the 1<sup>st</sup>-year ENSO properties and the associated SST conditions in the neighboring Indian/Atlantic Oceans and subtropical North Pacific to predict the subsequent ENSO evolution pattern.

There are a few related issues that are not addressed in this study but require further understanding. Firstly, if the positive feedbacks from the intra-basin interactions continue in the second year, multi-year ENSO events can persist for many years. Why did we not often observe such long-lasting multi-year events and what are the main processes responsible for the termination of these events? Aside from the negative feedbacks provided by the inter-basin interactions, stochastic/random extreme weather events or extratropical atmospheric variability outside the tropics may also contribute to the demise of these events. Secondly, it is known that a similar PMM mode exists in the southern hemisphere, which is referred to as the SPMM<sup>67</sup>. Previous studies suggested that the SPMM can affect ENSO’s location by triggering EP type events as it influences SSTs in the tropical eastern Pacific<sup>67,68</sup>. It is possible that the SPMM can also affect ENSO’s evolution pattern through intra-basin interactions between the tropical and subtropical South Pacific Oceans. Further studies are required to find out whether or not ENSO events can activate the

SPMM and if the associated intra-basin interactions produce positive or negative ENSO feedbacks on the events. Another important issue not addressed in the present study is whether there is any low-frequency variation in the occurrence ratio of single- and multi-year ENSO events, and if so, how the variation is linked to the low-frequency variability in the Indian, Pacific, and Atlantic Oceans. Also, since our study suggests that convective responses to ENSO SSTAs are a key to determine whether the inter- or intra-basin interactions should be activated to produce diverse ENSO evolution patterns, convection modulated climate indices (such as the ELI<sup>69</sup> and the InFACT<sup>70</sup>) may be particularly useful in helping further studies on ENSO complexity. Finally, the thresholds of the key factors identified in this study are likely model-dependent due to the fact that many contemporary climate models fail to simulate complex ENSO behaviors<sup>27</sup>. A thorough study that provides precise, quantitative information on the thresholds of the key factors simulated in other climate model outcomes (e.g., CMIP5/6 models) is therefore necessary.

## METHODS

### Observational data and identifying ENSO events

For the observational analysis, we used the Hadley Centre Sea Ice and Sea Surface Temperature, version 1.1 (HadISSTv1.1)<sup>71</sup> data that covers the period from 1871 to the present on a  $1^\circ \times 1^\circ$  global grid. The HadISSTv1.1 data uses reduced space optimal interpolation applied to SSTs from the Marine Data Bank, which are based on historical in situ ship and buoy observations, and the ICOADS through 1981 and a blend of in situ and adjusted satellite-derived SSTs after 1982. The missing grids are filled by optimal interpolation based on empirical orthogonal function analysis. Using the observational data, we identified 25 El Niños and 20 La Niñas during the analysis period for 1900–2020 (see Supplementary Table 1). An El Niño was defined when its first winter (i.e., November<sup>0</sup> to January<sup>1</sup>) Niño3.4 index is greater than 0.7 standard deviation (s.d.), which is 0.65 °C during 1900–2020. Likewise, a La Niña was defined when the winter Niño3.4 index is less than its  $-0.7$  s.d. The main results from the observational analysis did not change when using either the Niño3.4 index threshold of  $\pm 0.7$  s.d. ( $\pm 0.65$  °C) or 0.5 °C. Note that calendar months during the developing (decaying) year of the ENSO were denoted as months<sup>0(1)</sup>. Similarly, calendar months during the year before (after) the developing (decaying) year were denoted as months<sup>-1(2)</sup>.



## CESM1 and identifying ENSO events

Due to the limited number of ENSO events in observation (25 El Niños and 20 La Niñas for 1900–2020, this study), we utilized a 2200-year long-integrated model simulation from the Community Earth System Model, version 1 (CESM1)<sup>48</sup>. This CESM1 simulation, which is conducted with the nominal 1° horizontal resolution under preindustrial greenhouse gas concentrations, has been widely used in studies of ENSO since it produces one of the most realistic simulations of the ENSO phenomenon among global climate models by accurately reproducing the observed spatio-temporal characteristics of ENSO, such as its reoccurrence frequencies, amplitude ranges, spatial structures, and temporal evolutions as well as several key aspects of ENSO complexity<sup>23,26,28,51</sup>. We analyzed the model years 400–2200, during which the model exhibits a negligible SST trend ( $\sim 10^{-7}$  °C/100-yr) and a minor drift of global ocean temperature ( $\sim 0.005$  °C/100-yr). For the CESM1 analysis, the same criteria as in the observations were adopted to identify ENSO events, using  $\pm 0.7$  s.d. ( $\pm 0.79$  °C) of the first winter (i.e., November<sup>0</sup> to January<sup>1</sup>) Niño3.4 index. As a result, 314 El Niños and 346 La Niñas were identified in the model years for 400–2200.

## Determining single- and multi-year ENSO events

An ENSO event was determined as a single- or multi-year event by examining the signs of the Niño3.4 index during its second winter (i.e., November<sup>1</sup> to January<sup>2</sup>). An El Niño was considered to be a single-year event when its second winter Niño3.4 index is less or equal to zero; otherwise, it was considered to be a multi-year event. Conversely for La Niña, a single (multi)-year event was determined when the second winter Niño3.4 index is greater (less or equal to) than zero. Applying this method, we identified 14 single- and 11 multi-year El Niños in the observations (Fig. 1a; see Supplementary Table 1), and 168 single- and 146 multi-year El Niños in the CESM1 (Fig. 1e). Likewise, we identified 6 single- and 14 multi-year La Niñas in the observations (Fig. 1c; see Supplementary Table 1), and 98 single- and 248 multi-year La Niñas in the CESM1 (Fig. 1g).

## Definitions of climate indices used

A total of six climate indices based on SSTs (de-trended SST departures from their climatology with base periods of 1900–2020 for observation and 400–2200 for CESM1) were used in this study: the Niño3.4, Indian Ocean Dipole (IOD), Indian Ocean Basin (IOB), Tropical North Atlantic (TNA), Pacific Meridional Mode (PMM), and Zonal Location (ZL) indices. (i) The Niño3.4 index, which represents the intensity and temporal evolution of ENSO, is defined as SSTA averaged in the tropical central-to-eastern Pacific (i.e., 5°S–5°N and 170–120°W). (ii) The IOD index represents a zonally-dipole structure of SST variability in the Indian Ocean that prominently occurs on interannual time scale<sup>53</sup>. It is defined as the SSTA difference between the western Indian Ocean (i.e., 10°S–10°N and 50–70°E) and the southeastern Indian Ocean (i.e., 10°S–0 and 90–110°E) during boreal fall from September to November, in which IOD events usually peak. (iii) The IOB index represents a basin-scale uniform SST warming or cooling of the Indian Ocean that occurs on interannual to decadal time scales<sup>54</sup>. It is defined as the SSTA averaged in the Indian Ocean basin (i.e., 20°S–20°N and 40–115°E) during boreal spring from March to May, in which IOB events usually peak. (iv) The TNA index represents an SST variability of the subtropical North Atlantic that predominantly occurs on interannual time scales<sup>32,55</sup>. It is defined as the SSTA averaged over the TNA region in the North Atlantic (i.e., 10–20°N and 65–15°W) during boreal spring from March to May, in which TNA events typically peak. (v) The PMM index represents the interannual variability of coupled SST–surface wind pattern over the subtropical northeastern Pacific<sup>56,67</sup>. Motivated by the method

from Zhang et al.<sup>67</sup>, the PMM index is defined as the SSTA averaged over the subtropical northeastern Pacific region (i.e., 10–20°N and 165–115°W) during boreal spring from March to May, in which PMM events usually peak. Note that the method used in this study, with its simple computation, is essentially similar to the original SST-based PMM index suggested by Chiang & Vimont<sup>56</sup>. (vi) Finally, the ZL index is used to indicate whether the maximum center of an ENSO event is located more toward the tropical eastern or central Pacific during its mature stage. It is defined as the SSTA difference between the tropical eastern Pacific (i.e., 5°S–5°N and 160–100°W) and tropical central Pacific (i.e., 5°S–5°N and 150°E–160°W) during boreal winter from December to February, in which ENSO events usually mature. Since the index is defined by area-averaged SSTs, the central ENSO location it quantifies is not sensitive to the spatial resolution of the SST data (e.g., fine versus coarse resolutions).

## Significance test

The interquartile range (IQR) is conducted to examine whether a change from the seasonally-averaged climate indices in Fig. 2 is statistically significant. The IQR equals Q3 (i.e., 75<sup>th</sup> percentile) minus Q1 (i.e., 25<sup>th</sup> percentile) to obtain the spread taken up by the innermost 50% of the data. If the IQR is small, the data are mostly close to the median; otherwise, the data are more spread out from the median. The Student's *t* test is also carried out to determine whether the correlation coefficients computed in this study are statistically significant.

## Partial correlation

To achieve the pure relationship between the key property differences for El Niño and La Niña (developing-season intensity/maximum zonal location for El Niño and pre-onset Pacific condition/maximum zonal location for La Niña) and the seasonally-averaged key climate indices of IOD, IOB, TNA, and PMM, a partial correlation analysis is applied

$$r_{A(B|C)} = \frac{r_{AB} - r_{AC} * r_{CB}}{\sqrt{1 - r_{AC}^2} * \sqrt{1 - r_{CB}^2}} \quad (1)$$

where A, B, and C represent the three variables: climate index (such as the IOD index), key factor (such as developing-season intensity for El Niño), and the other key factor (such as maximum zonal location for El Niño), respectively. *r* denotes the correlation coefficient, and  $r_{A(B|C)}$  for partial correlation coefficient between the variable A and B, after the influence of C is removed from B.

## DATA AVAILABILITY

The HadISSTv1.1 data is available through the Met Office Hadley Center archives at <https://www.metoffice.gov.uk/hadobs/hadisst/>. The 2200-year CESM1 simulation is available via the Earth System Grid at <https://www.cesm.ucar.edu/projects/community-projects/LENS/data-sets.html>.

## CODE AVAILABILITY

Any relevant codes necessary to reproduce the results presented in this study are available from the authors upon request.

Received: 26 May 2022; Accepted: 30 September 2022;  
Published online: 14 November 2022

## REFERENCES

- Wyrtki, K. El Niño—the dynamic response of the equatorial Pacific Ocean to atmospheric forcing. *J. Phys. Oceanogr.* **5**, 572–584 (1975).
- Timmermann, A. et al. El Niño–Southern Oscillation complexity. *Nature* **559**, 535–545 (2018).

3. Kao, H. Y. & Yu, J. Y. Contrasting eastern-Pacific and central-Pacific types of ENSO. *J. Clim.* **22**, 615–632 (2009).
4. Yeh, S. W., Kug, J. S. & An, S. I. Recent progress on two types of El Niño: Observations, dynamics, and future changes. *Asia-Pac. J. Atmos. Sci.* **50**, 69–81 (2014).
5. Capotondi, A. et al. Understanding ENSO diversity. *Bull. Am. Meteor. Soc.* **96**, 921–938 (2015).
6. Wang, C., Deser, C., Yu, J. Y., DiNezio, P., & Clement, A. El Niño and southern oscillation (ENSO): a review. In *Coral Reefs of the Eastern Tropical Pacific*, Eds., Vol. 8, 85–106 (Springer, 2017).
7. Yu, J. Y., Wang, X., Yang, S., Paek, H., & Chen, M. *The changing El Niño–Southern Oscillation and associated climate extremes*, 1–38 (John Wiley & Sons, Inc., 2017).
8. An, S. I., Tziperman, E., Okumura, Y. M., & Li, T. ENSO irregularity and asymmetry. In *El Niño Southern Oscillation in a changing climate*, Vol. 253, 153–172 (John Wiley & Sons, Inc., 2020).
9. Fang, X. H. & Mu, M. A three-region conceptual model for central Pacific El Niño including zonal advective feedback. *J. Clim.* **31**, 4965–4979 (2018).
10. Geng, T., Cai, W. & Wu, L. Two types of ENSO varying in tandem facilitated by nonlinear atmospheric convection. *Geophys. Res. Lett.* **47**, e2020GL088784 (2020).
11. Chen, N., Fang, X. & Yu, J. Y. A multiscale model for El Niño complexity. *npj clim. Atmos.* **5**, 1–13 (2022).
12. Chen, M., Yu, J. Y., Wang, X. & Chen, S. Distinct onset mechanisms of two subtypes of CP El Niño and their changes in future warming. *Geophys. Res. Lett.* **48**, e2021GL093707 (2021).
13. Ding, R. et al. Multi-year El Niño events tied to the North Pacific Oscillation. *Nat. Commun.* **13**, 3871 (2022).
14. Suarez, M. J. & Schopf, P. S. A delayed action oscillator for ENSO. *J. Atmos. Sci.* **45**, 3283–3287 (1988).
15. Jin, F. F. An equatorial ocean recharge paradigm for ENSO. Part I: conceptual model. *J. Atmos. Sci.* **54**, 811–829 (1997).
16. Kessler, William S. Is ENSO a cycle or a series of events? *Geophys. Res. Lett.* **29**, 40–44 (2002).
17. McPhaden, M. J. & Zhang, X. Asymmetry in zonal phase propagation of ENSO sea surface temperature anomalies. *Geophys. Res. Lett.* **36**, L13703 (2009).
18. Ohba, M. & Ueda, H. Role of nonlinear atmospheric response to SST on the asymmetric transition process of ENSO. *J. Clim.* **22**, 177–192 (2009).
19. Okumura, Y. M., Ohba, M., Deser, C. & Ueda, H. A proposed mechanism for the asymmetric duration of El Niño and La Niña. *J. Clim.* **24**, 3822–3829 (2011).
20. An, S. I. & Kim, J. W. Role of nonlinear ocean dynamic response to wind on the asymmetrical transition of El Niño and La Niña. *Geophys. Res. Lett.* **44**, 393–400 (2017).
21. Fang, S. W. & Yu, J. Y. A control of ENSO transition complexity by tropical Pacific mean SSTs through tropical-subtropical interaction. *Geophys. Res. Lett.* **47**, e2020GL087933 (2020).
22. Chen, J. et al. Tropical and subtropical Pacific sources of the asymmetric El Niño–La Niña decay and their future changes. *Geophys. Res. Lett.* **49**, e2022GL097751 (2022).
23. Kim, J. W. & Yu, J. Y. Understanding reintensified multiyear El Niño events. *Geophys. Res. Lett.* **47**, e2020GL087644 (2020).
24. Lee, S. K. et al. Spring persistence, transition, and resurgence of El Niño. *Geophys. Res. Lett.* **41**, 8578–8585 (2014).
25. Yu, J. Y. & Fang, S. W. The distinct contributions of the seasonal footprinting and charged-discharged mechanisms to ENSO complexity. *Geophys. Res. Lett.* **45**, 6611–6618 (2018).
26. Wu, X., Okumura, Y. M. & DiNezio, P. N. What controls the duration of El Niño and La Niña events? *J. Clim.* **32**, 5941–5965 (2019).
27. Fang, S. W. & Yu, J. Y. Contrasting transition complexity between El Niño and La Niña: observations and CMIP5/6 models. *Geophys. Res. Lett.* **47**, e2020GL088926 (2020).
28. Kim, J. W. & Yu, J. Y. Evolution of subtropical Pacific-onset El Niño: how its onset location controls its decay evolution. *Geophys. Res. Lett.* **48**, e2020GL091345 (2021).
29. Cai, W. et al. Pantropical climate interactions. *Science* **363**, eaav4236 (2019).
30. Wang, J. Z. & Wang, C. Joint boost to super El Niño from the Indian and Atlantic oceans. *J. Clim.* **34**, 4937–4954 (2021).
31. Kug, J. S. & Kang, I. S. Interactive feedback between ENSO and the Indian Ocean. *J. Clim.* **19**, 1784–1801 (2006).
32. Ham, Y. G., Kug, J. S., Park, J. Y. & Jin, F. F. Sea surface temperature in the north tropical Atlantic as a trigger for El Niño/Southern Oscillation events. *Nat. Geosci.* **6**, 112–116 (2013).
33. Wang, L., Yu, J. Y. & Paek, H. Enhanced biennial variability in the Pacific due to Atlantic capacitor effect. *Nat. Commun.* **8**, 1–7 (2017).
34. Okumura, Y. M. ENSO diversity from an atmospheric perspective. *Curr. Clim. Change Rep.* **5**, 245–257 (2019).
35. Chen, J. et al. Unusual rainfall in southern China in decaying August during extreme El Niño 2015/16: Role of the western Indian Ocean and north tropical Atlantic SST. *J. Clim.* **31**, 7019–7034 (2018).
36. Chen, M., Yu, J. Y., Wang, X. & Jiang, W. The changing impact mechanisms of a diverse El Niño on the western Pacific subtropical high. *Geophys. Res. Lett.* **46**, 953–962 (2019).
37. Park, J. H., Li, T., Yeh, S. W. & Kim, H. Effect of recent Atlantic warming in strengthening Atlantic–Pacific teleconnection on interannual timescale via enhanced connection with the Pacific meridional mode. *Clim. Dyn.* **53**, 371–387 (2019).
38. Izumo, T. et al. Influence of the state of the Indian Ocean Dipole on the following year's El Niño. *Nat. Geosci.* **3**, 168 (2010).
39. An, S. I. & Kim, J. W. ENSO transition asymmetry: Internal and external causes and intermodel diversity. *Geophys. Res. Lett.* **45**, 5095–5104 (2018).
40. Yu, J. Y., Kao, H. Y. & Lee, T. Subtropics-related interannual sea surface temperature variability in the central equatorial Pacific. *J. Clim.* **23**, 2869–2884 (2010).
41. Yu, J. Y. & Kim, S. T. Relationships between extratropical sea level pressure variations and the central Pacific and eastern Pacific types of ENSO. *J. Clim.* **24**, 708–720 (2011).
42. Su, J., Zhang, R., Rong, X., Min, Q. & Zhu, C. Sea surface temperature in the subtropical Pacific boosted the 2015 El Niño and hindered the 2016 La Niña. *J. Clim.* **31**, 877–893 (2018).
43. Di Lorenzo, E. et al. ENSO and meridional modes: a null hypothesis for Pacific climate variability. *Geophys. Res. Lett.* **42**, 9440–9448 (2015).
44. Lyu, K., Yu, J. Y. & Paek, H. The influences of the Atlantic multidecadal oscillation on the mean strength of the North Pacific subtropical high during boreal winter. *J. Clim.* **30**, 411–426 (2017).
45. Stuecker, M. F. Revisiting the Pacific meridional mode. *Sci. Rep.* **8**, 1–9 (2018).
46. Xie, S. P. & Philander, S. G. H. A coupled ocean-atmosphere model of relevance to the ITCZ in the eastern Pacific. *Tellus A* **46**, 340–350 (1994).
47. Anderson, B. T. & Perez, R. C. ENSO and non-ENSO induced charging and discharging of the equatorial Pacific. *Clim. Dyn.* **45**, 2309–2327 (2015).
48. Kay, J. E. et al. The Community Earth System Model (CESM) large ensemble project: a community resource for studying climate change in the presence of internal climate variability. *Bull. Am. Meteor. Soc.* **96**, 1333–1349 (2015).
49. Yeh, S. W., Jo, H. S., Hyun, S. H., Cai, W. & Ham, Y. G. Role of the eastern subtropical North Pacific Ocean on the El Niño's transition processes. *Clim. Dyn.* **56**, 1285–1301 (2021).
50. Yeh, S. W. et al. ENSO atmospheric teleconnections and their response to greenhouse gas forcing. *Rev. Geophys.* **56**, 185–206 (2018).
51. DiNezio, P. N., Deser, C., Okumura, Y. & Karspeck, A. Predictability of 2-year La Niña events in a coupled general circulation model. *Clim. Dyn.* **49**, 4237–4261 (2017).
52. Larson, S. M. & Pegion, K. Do asymmetries in ENSO predictability arise from different recharged states? *Clim. Dyn.* **54**, 1507–1522 (2020).
53. Saji, N. H., Goswami, B. N., Vinayachandran, P. N. & Yamagata, T. A dipole mode in the tropical Indian Ocean. *Nature* **401**, 360 (1999).
54. Yang, J., Liu, Q., Xie, S. P., Liu, Z. & Wu, L. Impact of the Indian Ocean SST basin mode on the Asian summer monsoon. *Geophys. Res. Lett.* **34**, L02708 (2007).
55. Saravanan, R. & Chang, P. Interaction between tropical Atlantic variability and El Niño–Southern oscillation. *J. Clim.* **13**, 2177–2194 (2000).
56. Chiang, J. C. & Vimont, D. J. Analogous Pacific and Atlantic meridional modes of tropical atmosphere–ocean variability. *J. Clim.* **17**, 4143–4158 (2004).
57. Yu, J. Y. & Kao, H. Y. Decadal changes of ENSO persistence barrier in SST and ocean heat content indices: 1958–2001. *J. Geophys. Res. Atmos.* **112**, D13106 (2007).
58. Sud, Y. C., Walker, G. K. & Lau, K. M. Mechanisms regulating sea-surface temperatures and deep convection in the tropics. *Geophys. Res. Lett.* **26**, 1019–1022 (1999).
59. Trenberth, K. E. et al. Progress during TOGA in understanding and modeling global teleconnections associated with tropical sea surface temperatures. *J. Geophys. Res. Oceans* **103**, 14291–14324 (1998).
60. Alexander, M. A. et al. The atmospheric bridge: the influence of ENSO teleconnections on air–sea interaction over the global oceans. *J. Clim.* **15**, 2205–2231 (2002).
61. Alexander, M. & Scott, J. The influence of ENSO on air–sea interaction in the Atlantic. *Geophys. Res. Lett.* **29**, 46–1 (2002).
62. Zou, Y., Yu, J. Y., Lee, T., Lu, M. M. & Kim, S. T. CMIP5 model simulations of the impacts of the two types of El Niño on US winter temperature. *J. Geophys. Res. Atmos.* **119**, 3076–3092 (2014).
63. Yu, J. Y., Paek, H., Saltzman, E. S. & Lee, T. The early-1990s change in ENSO-PSA-SAM relationships and its impact on Southern Hemisphere climate. *J. Clim.* **28**, 9393–9408 (2015).
64. Iwakiri, T. & Watanabe, M. Mechanisms linking multi-year La Niña with preceding strong El Niño. *Sci. Rep.* **11**, 1–11 (2021).
65. Barnston, A. G., Tippett, M. K., Ranganathan, M. & L'Heureux, M. L. Deterministic skill of ENSO predictions from the North American Multimodel Ensemble. *Clim. Dyn.* **53**, 7215–7234 (2019).

66. Wu, X., Okumura, Y. M., Deser, C. & DiNezio, P. N. Two-year dynamical predictions of ENSO event duration during 1954–2015. *J. Clim.* **34**, 4069–4087 (2021).
67. Zhang, H., Clement, A. & Di Nezio, P. The South Pacific meridional mode: a mechanism for ENSO-like variability. *J. Clim.* **27**, 769–783 (2014).
68. Amaya, D. J. The Pacific meridional mode and ENSO: a review. *Curr. Clim. Change Rep.* **5**, 296–307 (2019).
69. Williams, I. N. & Patricola, C. M. Diversity of ENSO events unified by convective threshold sea surface temperature: a nonlinear ENSO index. *Geophys. Res. Lett.* **45**, 9236–9244 (2018).
70. Xie, R., Mu, M. & Fang, X. New indices for better understanding ENSO by incorporating convection sensitivity to sea surface temperature. *J. Clim.* **33**, 7045–7061 (2020).
71. Rayner, N. A. A. et al. Global analyses of sea surface temperature, sea ice, and night marine air temperature since the late nineteenth century. *J. Geophys. Res. Atmos.* **108**, 4407 (2003).

## ACKNOWLEDGEMENTS

The authors thank the editor Dr. Fred Kucharski and the three anonymous reviewers whose valuable comments and suggestions greatly improved this study. The authors are also very grateful to all observational data providers and the CESM1 Large Ensemble Community Project provided by NSF/CISL/Yellowstone. A special thanks to Gabrielle N. Bustamante-Kim for the noteworthy assistance on polishing the writing of this manuscript. This research was supported by NSF Climate and Large-Scale Dynamics Program under grants AGS-1833075 and 2109539.

## AUTHOR CONTRIBUTIONS

J.-W.K. and J.-Y.Y. designed the research. J.-W.K. performed the analyses and wrote a draft of the paper. J.-W.K. and J.-Y.Y. discussed the results and wrote the manuscript.

## COMPETING INTERESTS

The authors declare no competing interests.

## ADDITIONAL INFORMATION

**Supplementary information** The online version contains supplementary material available at <https://doi.org/10.1038/s41612-022-00305-y>.

**Correspondence** and requests for materials should be addressed to Ji-Won Kim.

**Reprints and permission information** is available at <http://www.nature.com/reprints>

**Publisher's note** Springer Nature remains neutral with regard to jurisdictional claims in published maps and institutional affiliations.



**Open Access** This article is licensed under a Creative Commons Attribution 4.0 International License, which permits use, sharing, adaptation, distribution and reproduction in any medium or format, as long as you give appropriate credit to the original author(s) and the source, provide a link to the Creative Commons license, and indicate if changes were made. The images or other third party material in this article are included in the article's Creative Commons license, unless indicated otherwise in a credit line to the material. If material is not included in the article's Creative Commons license and your intended use is not permitted by statutory regulation or exceeds the permitted use, you will need to obtain permission directly from the copyright holder. To view a copy of this license, visit <http://creativecommons.org/licenses/by/4.0/>.

© The Author(s) 2022